Current Filamentation Instability in Laser Wakefield Accelerators

C. M. Huntington,[1,*] A. G. R. Thomas,[2] C. McGuffey,[2] T. Matsuoka,[2,†] V. Chvykov,[2] G. Kalintchenko,[2] S. Kneip,[3] Z. Najmudin,[3] C. Palmer,[3] V. Yanovsky,[2] A. Maksimchuk,[2] R. P. Drake,[1] T. Katsouleas,[4] and K. Krushelnick[2]

[1]*Atmospheric, Oceanic and Space Science, University of Michigan, Ann Arbor, Michigan, 48103, USA*
[2]*Center for Ultrafast Optical Science, The University of Michigan, Ann Arbor, Michigan 48109, USA*
[3]*The Blackett Laboratory, Imperial College London, London, SW7 2BZ, United Kingdom*
[4]*Platt School of Engineering, Duke University, Durham, North Carolina, 27708, USA*

(Received 16 November 2010; published 8 March 2011)

Experiments using an electron beam produced by laser-wakefield acceleration have shown that varying the overall beam-plasma interaction length results in current filamentation at lengths that exceed the laser depletion length in the plasma. Three-dimensional simulations show this to be a combination of hosing, beam erosion, and filamentation of the decelerated beam. This work suggests the ability to perform scaled experiments of astrophysical instabilities. Additionally, understanding the processes involved with electron beam propagation is essential to the development of wakefield accelerator applications.

DOI: 10.1103/PhysRevLett.106.105001 PACS numbers: 52.38.Kd, 52.35.−g, 52.72.+v, 98.70.Rz

In a laser-wakefield accelerator, electron bunches can be accelerated to relativistic energies by ''surfing'' on electron-plasma waves generated by an ultraintense laser pulse as it propagates through a low-density plasma [1]. As the leading edge of the laser ionizes the gas, the high electric field gradients expel the electrons via the ponderomotive force, leaving behind a bare ion cavity. The resulting electron density profile resembles a near-spherical ''bubble'' following the laser pulse. The space-charge separation at the rear of the bubble can produce electric fields of tens or hundreds of GeV/m and can be used to accelerate trapped electrons to near the speed of light. These electric field strengths are significantly higher than those used in traditional radio-frequency cavities, and for this reason laser-wakefield accelerators are a promising avenue in the search for next-generation accelerators.

To achieve the greatest energy gain, it is necessary to increase the length of the accelerating region, maximizing the distance over which electrons can extract energy from the driving laser pulse. However, as the laser pulse propagates it continuously loses energy to the plasma in generating the wakefield. The length over which the laser pulse can sustain a wakefield is given by the pump depletion length, and in the nonlinear 3D regime this is given as $L_{pd} = (n_{cr}/n_0)c\tau_p$, where $n_{cr} = \omega_0^2 m_e \epsilon_0/e^2$ is the critical density for a laser of angular frequency ω_0, τ_p is the pulse duration, and n_p is the unperturbed plasma electron density [2].

If the length of the gas target used exceeds the pump depletion length, the electron beam will subsequently propagate through an approximately uniform, quasineutral plasma, instead of the bare ion channel generated by the plasma bubble. As well as driving its own wakefield [3], the electron beam may be susceptible to filamentation and propagation instabilities. Weibel [4] first discovered that an electron distribution with an anisotropic temperature can lead to the growth of self-excited transverse electromagnetic waves. A related transverse instability for relativistic electron beams is the current filamentation instability [5], which occurs when the magnetic field generated by the beam causes an initial seed modulation in the transverse current profile to be amplified by the Lorentz force, $\mathbf{j} \times \mathbf{B}$. The evolving current filaments produced by these instabilities lead to a densely tangled magnetic field structure which serves to ''jitter'' the electrons. In astrophysics, observations of gamma-ray bursts can be characterized by the spectra of the long-duration afterglow, which may be the result of such jitter radiation [6,7].

Relativistic current filamentation has recently been observed in interactions between a laser pulse and a solid target [8]. The physics of the filamentation is governed by the size of the beam relative to the plasma skin depth, $\delta = c/\omega_p$, where $\omega_p = e^2 n_p/m_e\epsilon_0$. Return current flow will be entirely outside the beam for a transverse width less than a skin depth, but for larger beams it will be through the beam [9] and therefore lead to counterflowing electrons that will be susceptible to the filamentation instability. Additionally, for high current densities, wakefield excitation can also contribute to hosing of the beam and beam breakup [10,11].

To investigate current filamentation, we conducted experiments using the 30 fs, $\lambda_0 = 0.8$ μm HERCULES laser at the University of Michigan [12] to generate relativistic electron beams. The laser wave front was corrected using a deformable mirror, and the beam was focused to approximately 10 μm FWHM spot size using an $f/10$ off-axis parabola. Shots were taken with 28 ± 3 TW peak power with a focused intensity of 4×10^{19} W/cm^2, resulting in a normalized vector potential $a_0 = 4.4$. The pulse was focused onto the front edge of an expanding helium gas plume created by the flow of gas through a supersonic conical nozzle. To vary the length of the plasma channel

 © 2011 American Physical Society

a range of gas nozzles were used, with diameters of 0.5, 1, 2, 3, and 5 mm. The set of nozzles were shot on sequential shot days, during which the laser parameters and major alignment remained the same. The repeatability of the pulse was checked by imaging the laser immediately before beginning the experiment. The backing pressure was varied during each shot cycle, with electron densities ranging from 1×10^{19}–2.6×10^{19} during the experiment.

To measure electron density and image the plasma channel structure, we employed a transverse interferometer beam orthogonal to the main laser pulse direction. The length of the plasma column was to be measured directly from a calibrated image, while the density measurement was made via Abel inversion of the interferometer image. The error associated with the Abel inversion process was measured to be approximately 10% in the density range of interest.

The energy of the electron beam was measured with a spectrometer using a 0.8 T sector magnet which dispersed the beam onto a scintillator screen. When the magnet was removed from the beam path, a beam profile image was recorded by a second screen placed on axis approximately 90 cm beyond the gas nozzle, providing a measure of the electron beam divergence. A removable optical imaging system was in place to monitor the laser light after passing through the plasma. This confirmed that the laser pulse was self-focused through the gas jet and did not filament in a manner that would affect the observed electron beam.

Reconstructed density maps confirmed the increasing plasma interaction length as the nozzle diameter increased. The narrowest nozzle used was 500 μm and produced a plasma channel of nearly 380 μm. At this length a single electron beam with a broad energy between 20 and 70 MeV was consistently produced (51 of 62 shots). The beam was elliptical and showed no evidence of multiple bunches [Fig. 1(a)]. At this length beam loading has not yet occurred and injection at the back of the bubble is continuous, resulting in the broad energy spectrum observed [13]. From the scalings described previously, the plasma channel is too short for maximum acceleration and the electron population does not rotate in phase space, explaining the low maximum energy achieved with this nozzle.

Using a 1 mm conical nozzle to lengthen the plasma channel, electron beams were often produced with broad spectra, though monoenergetic beams were also observed. The channel was sustained for 880 μm, which was long enough to accelerate the electron beam to approximately 190 MeV. This can occur when electrons have gained maximum energy from the laser-sustained plasma wave, but before dephasing slows the beam.

The 2 mm nozzle produced a plasma channel of approximately 1800 μm. The electron spectrometer reveals quasimonoenergetic or dual-peaked spectra with initial signs of transverse beam spread. Shown in Fig. 2(c) is an energy spectrum from this plasma length. The profile images show

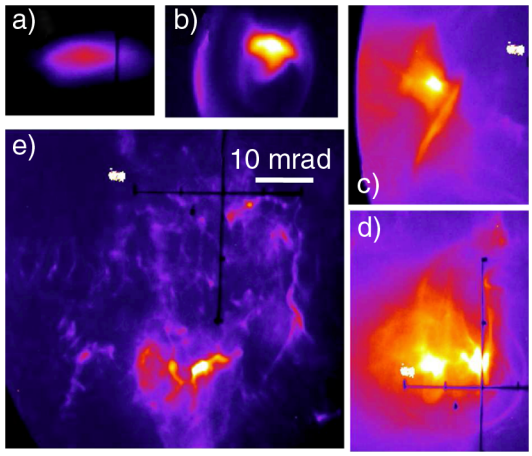

FIG. 1 (color online). Representative electron beam profile images in the transverse ($x_2 - x_3$, horizontal-vertical) plane for nozzle lengths (a) 500 μm, (b) 1 mm, (c) 2 mm, (d) 3 mm, (e) 5 mm. The spatial scale shown applies in both vertical and horizontal axes and is equal for all subfigures.

either one or two beam main filaments surrounded by a disperse ''halo'' [Fig. 1(c)]. Because these electrons are not seen on the spectrometer, they are likely below 20 MeV and thus outside of the spectrometer energy detection range. The pump depletion length can be estimated at 1.1 mm for an electron density of 1.4×10^{19} cm^{-3}, which was the density observed for this nozzle. Consequently, significant charge at higher energies was not observed for lengths longer than this nozzle in this experiment.

At 3 mm the beam showed increased divergence [Fig. 1(d)] and a broad energy spectrum [Fig. 2(d)]. It is expected that after propagation through this length of gas

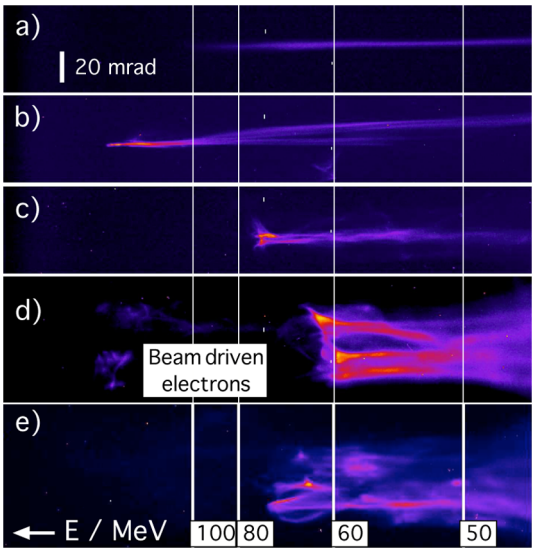

FIG. 2 (color online). Representative electron spectrometer images for nozzles of length (a) 500 μm, (b) 1 mm, (c) 2 mm, (d) 3 mm, (e) 5 mm. The maximum energy shown in (b) is approximately 190 MeV.

target the laser pulse is depleted far below the intensity necessary to drive a wake. As a result, the profile images showed a halo on all shots. This effect is evident in the spectrometer images as well, where filaments with nearly equal energy are displaced in space [vertical separation in Figs. 2(d) and 2(e)]. In this case the leading electron bunch is propagating through the He plasma and begins to drive its own plasma wake. This bunch becomes susceptible to current filamentation instabilities as the fast electron beam is neutralized by upstream electrons. There is also evidence of small bunches of electrons with energies near 200 MeV, consistent with beam driven acceleration of a small portion of the rear of the bunch or trapping of secondary bunches, as observed in [14].

The largest diameter nozzle used was 5 mm, which created a plasma channel of nearly 4500 μm. The beam profile at this stage is highly filamented, with multiple bunches evident in the beam profile [Fig. 1(e)]. These filaments are qualitatively different from structures seen in the shorter plasma lengths. Integrating the total charge collected on the profile scintillation screen suggests a saturation in the number of electrons injected, shown in Fig. 3. The large halo observed in the profile image results from beam erosion and is quantified by the decrease in localized charge (charge in primary filaments) at plasma lengths beyond the dephasing length (Fig. 3). Modifications to the plasma channel profile at this length affected electron production, but beam filamentation was evident whenever electrons were observed, regardless of the details of the plasma profile.

A simple estimate of the growth rate Γ of the current filamentation instability for a homogenous relativistic beam of density n_b propagating through a plasma of density n_p with Lorentz factor $\gamma_b = 1/\sqrt{1-\beta_b^2}$ is $\Gamma = \omega_p \beta_b (n_b/\gamma n_p)^{1/2}$ [5]. The main filament is not susceptible to the instability as it is both very relativistic,

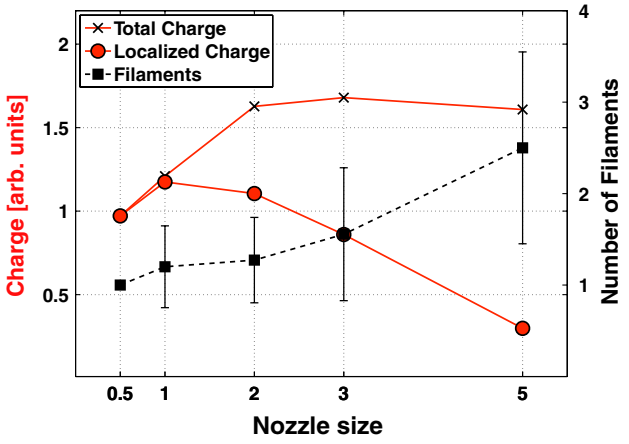

FIG. 3 (color online). Total charge, localized charge, and number of filaments per image. Localized charge is defined as integrated intensity when electrons outside of filament bunches are excluded.

$\gamma_b > 100$, and has small transverse extent compared with c/ω_p. However, for the halo, which has particle energies below 20 MeV, a larger divergence, and a beam density not far below the background density, the growth rate can be estimated, for $\gamma = 16$ and $n_b/n_p = 1/100$, as $\Gamma = \omega_p/40$. The length propagated to achieve 8 e-foldings, corresponding to a gain of 3000, is $50 \times 2\pi c/\omega_p$, or 500 μm for a density of 1.1×10^{19} cm^{-3}. This 1D estimate suggests that filamentation is qualitatively feasible given the parameters of this experiment. However, 3D effects and saturation of the instability will affect the quantitative degree of growth measured in experiment.

Three-dimensional particle-in-cell simulations of the interaction were performed using the OSIRIS 2.0 framework [15]. Simulation *A* modeled the propagation of Gaussian laser pulse with pulse duration 29 fs FWHM, beam waist $w_0 = 10$ μm, and normalized vector potential of $a_0 = 4$ in a helium plasma with a fully ionized electron density of $0.005 n_c$. The density profile consisted of a vacuum region followed by a short linear ramp of length 63.7 μm and subsequently a constant density. This simulation was run using two particles per cell with a resolution of 6π cells per λ_0 in the propagation direction (x_1) and $2\pi/3$ cells per λ_0 in both directions perpendicular to propagation (x_2 and x_3).

Figures 4(a) and 4(b) show the longitudinal current density in a window moving at c, after propagation of (a) 0.84 mm and (b) 2.9 mm of the laser. In 4(a), the laser pulse drives a region of strong electron cavitation, forming an accelerating bubble structure. Significant electron charge is self-trapped and accelerated in the bubble to an energy exceeding 300 MeV in a quasimonoenergetic peak with a broad energy spread. Depletion of the laser driver occurs subsequently, and after 2.9 mm propagation [4(b)] the laser no longer generates a wakefield. However, the electron beam driver itself now generates its own wakefield through space-charge repulsion [3]. Acceleration of a small portion of the rear of the electron bunch to energies in excess of 400 MeV and also erosion of the electron beam driver head occurs, the latter resulting in a lower energy and more diffuse cloud of electrons, as seen in the experiments. The beam driven wakefield is unstable to the electron beam hosing instability in an ion channel [10,11], which ultimately results in filamentation and destruction of the beam structure.

By 3.5 mm the beam structure is sufficiently fragmented and/or eroded that the beam charge profile is indistinguishable from noise due to the reduction of its density to below the background level. Phase spaces indicate that there is a significant population of the original beam in the diffuse cloud with an average forward momentum distribution below 20 MeV. To model the behavior of this low energy halo, simulation *B* was run without a laser pulse, with a resolution of $\pi/3$ cells per λ_0 in x_1 and π cells per λ_0 in x_2, x_3. An initially spatially uniform electron beam of density $0.0005 n_c$ with a Gaussian temporal profile of

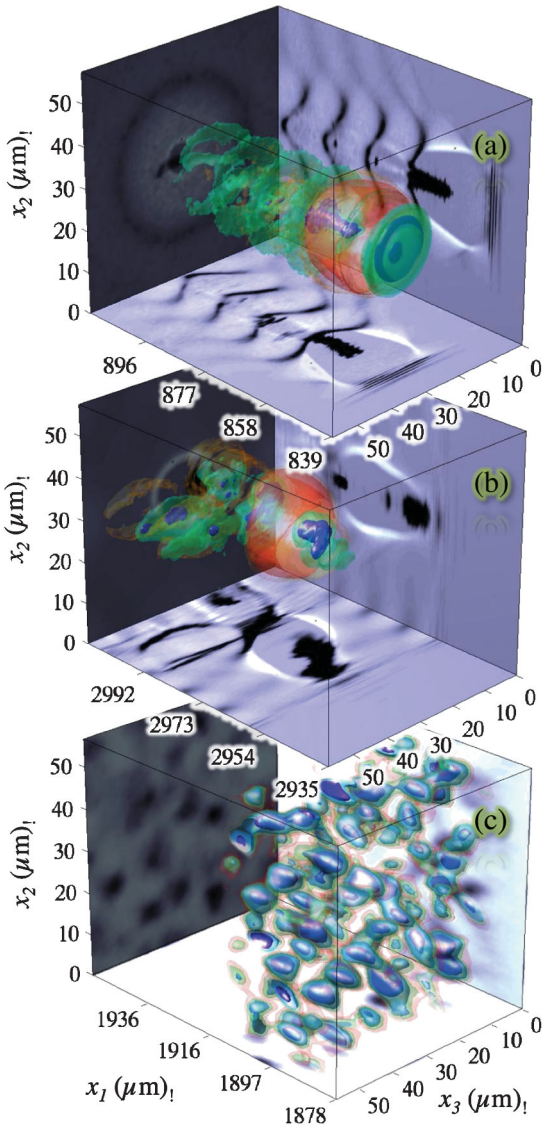

FIG. 4 (color). Isosurface plots from OSIRIS 2.0 [15] simulations in a box moving at c. Side panels display slices through the center of the box. (a),(b) The forward current density in simulation A after propagating (a) 0.84 mm and (b) 2.9 mm. Isosurfaces are at (blue, green) 10% and 2% of minimum and (red, orange) 25% and 50% of maximum current. (c) Final charge density of the electron beam of simulation B, with isosurfaces at 75%, 70%, 65%, and 50% maximum.

duration $150/\omega_0$, average momentum $p_{x_1} = 20m_e c$, and a thermal distribution with $\Delta p_{x_1} = 20m_e c$, $\Delta p_{x_{2,3}} = 2m_e c$ was propagated in a uniform plasma of density $n = 0.005n_c$. The beam density and temporal profile were taken to be similar to those observed in simulation A at 3.5 mm. Being a separate population from the background electrons allowed the easy identification of structures formed in the beam from filamentation instabilities. After 1.9 mm of beam propagation, the instability had saturated and the area A of the filaments projected onto a 2D grid were analyzed using a threshold image at half maximum intensity. Their diameter, defined as $d = 2\sqrt{A/\pi}$, was found to vary between $0.57c/\omega_p$ and $1.74c/\omega_p$ with a mean of $1.07c/\omega_p$, consistent with the current filamentation instability.

At the longer gas target lengths, these experiments demonstrate a potential test bed for laboratory astrophysics experiments on jitter radiation with relevance to gamma-ray-burst afterglow. X-ray measurements under these conditions [16] also showed an increase in x-ray flux for up to a 10 mm nozzle, beyond the point where betatron radiation from the wakefield would be expected, indicating radiation generation in the filamented region. This will be reported on in a future paper. The sensitivity of the smaller target lengths highlight the narrow range of parameter space one must work in to achieve maximum electron acceleration before effects like dephasing, pump depletion, and current instabilities like hosing and filamentation degrade beam quality. Controlling these effects is also crucial to realizing laser-wakefield acceleration for next-generation particle accelerator schemes.

This work was supported by NSF through the Physics Frontier Center FOCUS (PHY-0114336) and NSF/DOE (PHY-09-03557). The authors would like to acknowledge the OSIRIS Consortium (UCLA, IST Portugal) for the use of the OSIRIS 2.0 framework. T. K. acknowledges support from USC that led to this work and NSF (PHY-09-36278).

*channing@umich.edu
†Present address: Japan Aerospace Exploration Agency, Sagamihara Tyuouku, Kanagawa, Japan.

[1] S. P. D. Mangles *et al.*, Nature (London) **431**, 535 (2004); C. G. R. Geddes *et al.*, Nature (London) **431**, 538 (2004); J. Faure *et al.*, Nature (London) **431**, 541 (2004).
[2] W. Lu *et al.*, Phys. Rev. ST Accel. Beams **10**, 061301 (2007).
[3] P. Chen, J. M. Dawson, R. W. Huff, and T. Katsouleas, Phys. Rev. Lett. **54**, 693 (1985).
[4] E. S. Weibel, Phys. Rev. Lett. **2**, 83 (1959).
[5] F. Califano, R. Prandi, F. Pegoraro, and S. V. Bulanov, Phys. Rev. E **58**, 7837 (1998).
[6] M. V. Medvedev, D. Lazzati, B. C. Morsony, and J. C. Workman, Astrophys. J. **666**, 339 (2007).
[7] M. V. Medvedev, Astrophys. Space Sci. **322**, 147 (2008).
[8] M. Tatarakis *et al.*, Phys. Rev. Lett. **90**, 175001 (2003).
[9] J. J. Su *et al.*, IEEE Trans. Plasma Sci. **15**, 192 (1987).
[10] E. S. Dodd *et al.*, Phys. Rev. Lett. **88**, 125001 (2002).
[11] S. Deng *et al.*, Phys. Rev. Lett. **96**, 045001 (2006).
[12] V. Yanovsky *et al.*, Opt. Express **16**, 2109 (2008).
[13] S. P. D. Mangles *et al.*, Phys. Plasmas **14**, 056702 (2007).
[14] F. S. Tsung *et al.*, Phys. Plasmas **13**, 056708 (2006).
[15] R. A. Fonseca *et al.*, in *Computational Science–ICCS 2002*, Lecture Notes in Computer Science Vol. 2331 (Springer, New York, 2002), p. 342.
[16] S. Kneip *et al.*, Nature Phys. **6**, 980 (2010).